ISSN 1063-7788, Physics of Atomic Nuclei, 2019, Vol. 82, No. 4, pp. 366–384. © Pleiades Publishing, Ltd., 2019.
Russian Text © The Author(s), 2019, published in Yadernaya Fizika, 2019, Vol. 82, No. 4, pp. 320–338.

NUCLEI
Theory

Results of Microscopic Self-Consistent Theory of Quasiparticle–Phonon Interaction in Nuclei

S. P. Kamerdzhiev[1)*], O. I. Achakovskiy[2)], S. V. Tolokonnikov[1),3)], and M. I. Shitov[1)]

Received December 25, 2018; revised December 25, 2018; accepted December 25, 2018

Abstract—A self-consistent approach in the problem of taking into account quasiparticle–phonon interaction provides a high predictive power and is free from adjustable parameters (this is of crucial importance for astrophysics). Moreover, it is consistent and makes it possible to take into account new effects. A brief survey of the results obtained within this approach on the basis of Skyrme or Fayans functionals by employing the smallness parameter g^2, where g is the phonon-production amplitudes, with allowance for tadpole effects is presented. The contribution of quasiparticle–phonon interaction to ground-state electromagnetic moments of odd nuclei; second-order anharmonic effects in g^2, including quadrupole moments of the first 2^+ and 3^- states and EL transitions between one-phonon states; third-order anharmonic effects; pygmy dipole and giant resonances; and the contribution of quasiparticle–phonon interaction to radiative properties of nuclear reactions are considered. For magic and semimagic nuclei, additional effects and structures arising in nuclear features because of quasiparticle–phonon interaction are discussed along with new—that is, three- and four-quasiparticle ground-state—correlations. Earlier unknown values of the above features, including the features of the pygmy dipole resonance in neutron-rich nickel isotopes, are predicted. It is shown that, in all of the aforementioned problems, the contributions of quasiparticle–phonon interaction is sizable, is of fundamental importance, and is necessary for explaining experimental data.

DOI: 10.1134/S1063778819040100

1. INTRODUCTION

The problem of including quasiparticle–phonon interaction in the microscopic theory of the nucleus has a long history that was full of interesting and important achievements [1, 2]. The fact of employing two phenomenological parameter sets that describe a nuclear mean field and an effective interaction (that is, single-particle and collective excitations) was the most important and the most characteristic point of this history. As was convincingly demonstrated in the studies of the Copenhagen school [1], these parameters could be determined from experimental data. However, a vigorous development of astrophysical lines of research in nuclear physics and additional needs for nuclear data revealed that information about the properties of nuclei and features of nuclear reactions are required for nearly all nuclides (there are approximately six to eight thousands of them), the overwhelming majority of which are unstable. For such nuclei, there are virtually no experimental data necessary for evaluating phenomenological parameters. Therefore, there arose an urgent need for developing microscopic approaches that would at least exclude the existence of two parameter sets by reducing them to one set. This set would make it possible to calculate both the nuclear mean field and the effective interaction—that is, the properties of both the ground state and excited states—at least in the region of relatively low (up to 30 or 40 MeV) energies (regions of pygmy and giant resonances). This goal was accomplished owing to the development of self-consistent microscopic approaches [3–5]. The self-consistent theory of finite Fermi systems (TFFS) [6] that employs the Fayans functional [7, 8] or the Skyrme functional [9] is one version of the aforementioned approaches.

As a matter of fact, microscopic approaches that take into account quasiparticle–phonon interaction within the non-self-consistent quasiparticle–phonon model [2] and within the Green's function formalism [10–12, 15] were developed earlier than the above methods or simultaneously with them. In the quasiparticle–phonon model, the quasiparticle–phonon interaction was taken into account in a unified way over the whole region of low energies,

[1)]National Research Center Kurchatov Institute, Moscow, 123182 Russia.
[2)]Leipunsky Institute of Physics and Power Engineering, Obninsk, Kaluga oblast, 249033 Russia.
[3)]Moscow Institute of Physics and Technology (State University), Dolgoprudnyi, Moscow oblast, 141700 Russia.
[*]E-mail: kamerdzhiev_sp@nrcki.ru

Table 1. Energies ω_3 (in MeV units) and probabilities $B(E3)\uparrow$ (in $e^2\mathrm{b}^3$ units) for the excitation of 3_1^- states in even tin isotopes (the experimental data on display were taken from [21])

A	ω_3	ω_3^{expt}	$B(E3)$	$B(E3)^{\mathrm{exp}}$
100	5.621	–	0.109	–
102	3.959	–	0.0565	–
104	3.643	–	0.0760	–
106	3.457	–	0.0901	–
108	3.350	–	0.0959	–
110	3.282	[2.459]	0.0996	–
112	3.221	2.355	0.102	0.087(12)
114	3.157	2.275	0.106	0.100(12)
116	3.100	2.266	0.106	0.127(17)
118	3.072	2.325	0.106	0.115(10)
120	3.069	2.401	0.112	0.115(15)
122	3.112	2.493	0.107	0.092(10)
124	3.208	2.614	0.103	0.073(10)
126	3.346	–	0.0973	–
128	3.547	–	0.0870	–
130	3.822	–	0.0784	–
132	4.572	[4.351]	0.129	–

but, in [6, 11], the properties of the ground state and low-lying one-phonon states were studied along with anharmonic effects involving two to three phonons, while the region of pygmy and giant resonances was treated on the basis of generalizing the standard theory of finite Fermi systems [12] to the case of taking into account quasiparticle–phonon interaction in the particle–hole propagators of TFFS [13–16].

The development and application of self-consistent approaches for problems that require the inclusion of quasiparticle–phonon interaction [17, 18] was the next step aimed at improving the description of available experimental data and at predicting new physics results associated with taking into account quasiparticle–phonon interaction. Here—in contrast to what we have within the self-consistent quasiparticle–phonon model [17]—there still exists a gap between approaches applied in the region of the ground state and low-lying excited states [6, 19], on one hand, and the approach in the region of the pygmy dipole resonance and giant dipole resonance (PDR and GDR) [18, 20], on the other hand.

The main body of the present article contains two parts that differ substantially from one another. In the first part, we describe the properties of the ground state and low-lying one-phonon states of magic and semimagic nuclei on the basis of the energy density functional in the Fayans form and analyze second- and third-order anharmonic effects in g^2, where g is the dimensionless phonon-production amplitude. The second part is devoted to analyzing and calculating nuclear features in the region of PDR and GDR energies. The respective calculations are performed self-consistently in the sense that the mean field and effective interaction are determined by employing Skyrme functionals. The features of nuclear reactions involving gamma rays (radiative-capture cross sections and spectra, as well as mean radiative widths) are also calculated in the second part. The conclusions drawn from the present analysis and some as-yet-unresolved problems are listed in the last section.

2. GROUND AND LOW-LYING STATES OF NUCLEI

We make use of the fact that there exists the small parameter

$$\alpha = \frac{|\langle 1\|g_{\mathrm{L}}\|2\rangle|^2}{(2j_1+1)\omega_{\mathrm{L}}^2} \ll 1 \qquad (1)$$

for magic [1] and semimagic nuclei, where g_s is the reduced matrix element for the amplitude of creation of a collective phonon with energy ω_{L}.

Basic TFFS equations [12] that describe, respectively, the polarizability of nuclei and the phonon-production amplitude have the following symbolic form:

$$\widehat{V} = \widehat{V_0} + \widehat{F}\widehat{A}\widehat{V}, \qquad (2)$$

$$\widehat{g_L} = \widehat{F}\widehat{A}\widehat{g}_{\mathrm{L}}, \qquad (3)$$

In these equations, all terms are matrices; F is an effective interaction amplitude that is calculated as the second variational derivative with respect to the density (for the scalar Landau–Migdal amplitude) or is taken from a description on numerous experimental data on magnetic moments (for the spin part of the interaction in F); and A is the particle–hole propagator, which is an integral of the products of various combinations of Green's functions: $G^p(\varepsilon)$ and $G^h(\varepsilon)$ and the anomalous Green's functions $F^{(1)}$ and $F^{(2)}$.

As an example, the results of self-consistent calculations of the properties of the first 3^- phonons in tin isotopes are presented in Table 1. These calculations were performed on the basis of self-consistent TFFS with parameters of the DF3-a Fayans functional. One can see that we have obtained a reasonable description for the energies of the first 3^-

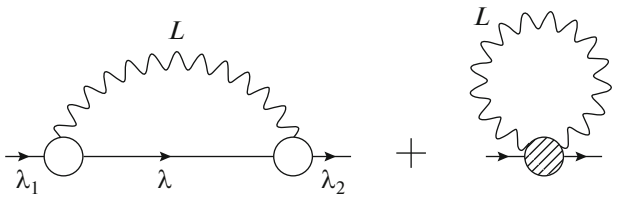

Fig. 1. Corrections of order g^2 to the mass operator in magic nuclei. The circles with one wavy line in the first term represent the phonon-production amplitude g, and the wavy lines stand for the phonon Green's function D. The solid lines represent the single-particle Green's functions. The second term is the phonon tadpole.

phonons and, what is of particular importance for g^2 effects, a good description of the reduced probabilities $B(E3)$.

In order to take into account corrections for quasiparticle–phonon interaction to single-particle features, it is necessary to consider such corrections to the mass operator shown in Fig. 1. In it, the pole diagram is supplemented with a nonpole diagram in the form of the so-called tadpole, which is the convolution of the phonon Green's function with $\delta_1 g_2$ (case of $1 = 2$). One can find this quantity as a variation of Eq. (3) for the amplitude g_2 in the field of phonon 1, and find that it satisfies the integral equation

$$g_{12} = \delta_1 F A g_2 + F(\delta_1 A) g_2 + F A g_{12}. \qquad (4)$$

In the case of $1 \neq 2$, we continue calling them tadpole effects. The corrections to the self-energy operator have the form

$$\delta\Sigma = \delta\Sigma^{\text{pole}} + \delta\Sigma^{\text{tad}}, \qquad (5)$$

$$\delta\Sigma^{\text{tad}} = \int \frac{d\omega}{2\pi i} \delta_L g_L D_L(\omega). \qquad (6)$$

Table 2. Contribution of quasiparticle–phonon interaction to neutron single-particle energies (in MeV units) in ^{208}Pb

λ	ε_λ [DF3-a + ph]	$\varepsilon_\lambda^{\text{exp}}$ [22]	ε_λ [RMF + ph]
$3d_{3/2}$	−1.171	−1.40	−0.63
$2g_{7/2}$	−1.426	−1.45	−1.14
$4s_{1/2}$	−1.483	−1.90	−0.92
$3d_{5/2}$	−2.023	−2.37	−1.39
$1j_{15/2}$	−2.483	−2.51	−1.84
$1i_{11/2}$	−2.327	−3.16	−3.30
$2g_{9/2}$	−3.924	−3.94	−3.29
$3p_{1/2}$	−7.549	−7.37	−7.68
$2f_{5/2}$	−8.316	−7.94	−8.66
$3p_{3/2}$	−8.338	−8.27	−8.26
$1i_{13/2}$	−8.905	−9.00	−9.10
$2f_{7/2}$	−10.059	−9.71	−9.71
$1h_{9/2}$	−10.535	−10.78	−11.78

2.1. Contribution of Quasiparicle–Phonon Interaction to Ground-State Properties

2.1.1. Single-particle features. In Fig. 2, theoretical single-particle levels obtained from self-consistent calculations with various functionals, including the HFB-17 Skyrme functional proposed most recently, are compared with experimental data. One can see that the theoretical spectrum is substantially less dense in the HFB-17 case than in the case of Fayans functionals, and the description of the experimental data is worse in the former case. The deviation from experimental data is due to the disregard of the contribution of quasiparticle–phonon interaction, and Table 2 gives the same levels calculated with allowance for quasiparticle–phonon interaction according to the equations

$$\delta\varepsilon_\lambda = Z_\lambda(\delta\Sigma^{\text{pole}}_{\lambda\lambda} + \delta\Sigma^{\text{tad}}_{\lambda\lambda}), \qquad (7)$$

$$Z_\lambda = \left(1 - \frac{\partial\Sigma_{\lambda\lambda}(\varepsilon)}{\partial\varepsilon}\bigg|_{\varepsilon=\varepsilon_\lambda}\right)^{-1} \qquad (8)$$

[the column containing the results of the calculations based on the relativistic-mean-field (RMF) method stands on the right]. One can see that the inclusion of the quasiparticle–phonon interaction improves substantially agreement with experimental data. A description of the same quality was obtained for other versions of the Fayans functional as well. The version of the RMF functional leads to substantially poorer results.

Table 3 gives two components of the correction for quasiparticle–phonon interaction in Eq. (5). One can see that the pole term is basically negative, while the nonpole term $\delta\varepsilon_\lambda^{\text{tad}}$ is always positive, so that, in the majority of cases, these corrections have opposite signs. Usually, the nonpole term is smaller in magnitude than the pole one, but, sometimes, the nonpole term makes a dominant contribution.

Figures 3 and 4 illustrate a more complicated case of self-consistent calculations, where single-particle features for semimagic nuclei have the form

$$\varepsilon_\lambda = \frac{\varepsilon_\lambda^{(0)} + M_\lambda^{\text{even}}(E_\lambda)}{1 + q_\lambda(E_\lambda)}, \qquad (9)$$

$$\Delta_\lambda = \frac{\Delta_\lambda^{(0)} + M_\lambda^{(1)}(E_\lambda)}{1 + q_\lambda(E_\lambda)}, \quad E_\lambda = \sqrt{\varepsilon_\lambda^2 + \Delta_\lambda^2},$$

Table 3. Pole and tadpole contributions of corrections for quasiparticle–phonon interaction from 3^- states to neutron single-particle energies (in MeV units) in ^{208}Pb

λ	$\delta\varepsilon_\lambda^{\text{pole}}$	$\delta\varepsilon_\lambda^{\text{tad}}$	$\delta\varepsilon_\lambda$
$3d_{3/2}$	−0.150	0.012	−0.137
$2g_{7/2}$	−0.142	0.061	−0.081
$4s_{1/2}$	−0.134	0.016	−0.118
$3d_{5/2}$	−0.147	0.023	−0.124
$1j_{15/2}$	−0.708	0.204	−0.504
$1i_{11/2}$	−0.058	0.198	0.140
$2g_{9/2}$	−0.244	0.076	−0.167
$3p_{1/2}$	−0.220	0.053	−0.167
$2f_{5/2}$	−0.186	0.094	−0.092
$3p_{3/2}$	−0.205	0.056	−0.149
$1i_{13/2}$	0.057	0.211	0.269
$2f_{7/2}$	0.724	0.091	0.815
$1h_{9/2}$	−0.014	0.197	0.184

where

$$q_\lambda = -\frac{M_\lambda^{\text{odd}}(E_\lambda)}{E_\lambda}, \tag{10}$$

while M^{even} and M^{odd} are, respectively, even and odd (in energy) parts of the pole term in Fig. 1 ($M = M^{\text{even}} + M^{\text{odd}}$).

The energies ε_λ and $\varepsilon_\lambda^{(0)}$ are reckoned from the respective chemical potentials μ and $\mu^{(0)}$. Here, we have employed the SLy4 Skyrme functional. Since the problem at hand is very complicated, the respective calculations were performed without taking into account corrections for tadpole effects in nuclei where pairing is present. So far, such corrections were only introduced in [27]. The contribution of quasiparticle–phonon interaction to the spectroscopic factor for the $2d_{3/2}$ level in ^{119}Sn is quite significant. Reasonable agreement with experimental data from [23–25] was obtained for stable tin isotopes. For unstable tin isotopes, the contribution of quasiparticle–phonon interaction leads to a strong fragmentation of single-particle levels, so that it is hardly possible to single out dominant levels. This is likely to be associated with a higher degree of collectivity of phonons in unstable than in stable nuclei, as can clearly be seen from the results of the calculations in Fig. 4 for *pairing-gap fragmentation* in tin isotopes. Good agreement with experimental data was obtained for the stable isotope ^{120}Sn upon taking into account the contribution of quasiparticle–phonon interaction [26]. The calculations considered here are a "self-consistent" continuation of the analysis performed in [28]. A rather comprehensive survey of the results on the role of quasiparticle–phonon interaction in the pairing gap can be found in [29] (see also [26, 30–36]).

2.1.2. Ground-state electromagnetic moments of odd nuclei. Within standard TFFS, electromagnetic moments of nuclei are determined in terms of the diagonal matrix element as

$$Q_\lambda = \langle\lambda|V|\lambda\rangle_{m=j}, \tag{11}$$

where λ is the odd-nucleon state and V is the normal component of the effective field. In the second order, corrections associated with quasiparticle–phonon interaction have the following symbolic form:

$$\begin{aligned}\delta^{(2)}V_{\lambda_1\lambda_2} \equiv \delta^2 V_{12} \\ = (\delta^2\phi_1 V\phi_2) + (\phi_1 V\delta^2\phi_2) + (\delta^1\phi_2 V\delta^1\phi_1) \\ + (\phi_2, \delta^2 V\phi_1) + (\delta^1\phi_2\delta^1 V\phi_1) + (\phi_2\delta^1 V\delta^1\phi_1).\end{aligned} \tag{12}$$

These corrections are called and are shown graphically in Fig. 5. In magic nuclei, a dominant correction stems from the 3_1^- phonon, while, in semimagic ones, it is due to the 2_1^+ phonon. The main results of the present calculations is a very strong compensation of the diagram in Fig. 5*c* (effect of phonon-induced interaction) and the two pole diagrams in Fig 5*a*. The remaining corrections then make a sizable contribution. The results obtained by calculating them are shown in Fig. 6. One can clearly see that the corrections for quasiparticle–phonon interaction improve substantially agreement with experimental data [37]. For more detailed results, the interested reader is referred to the studies reported in [30, 38–43].

2.2. Second-Order Anharmonic Effects

Anharmonic effects, which were qualitatively studied in low-energy nuclear physics, can be partitioned into second- and third-order effects in the phonon-production amplitude g if a relatively weak anharmonicity associated with the small parameter in (1) is assumed (in the following, such effects are referred to as, respectively, g^2 and g^3 effects). This means that the problem at hand is solved in a step-by-step way: first, phonons are constructed, whereupon their interactions are considered.

Anharmonic corrections of order g^2 for magic nuclei were studied long ago within nuclear field theory (NFT) [1] and by the Green's function method. For nuclei where pairing is present, such corrections were studied within the NFT framework, by the Green's function method, and within the consistent Hamiltonian approach implemented on the basis of the

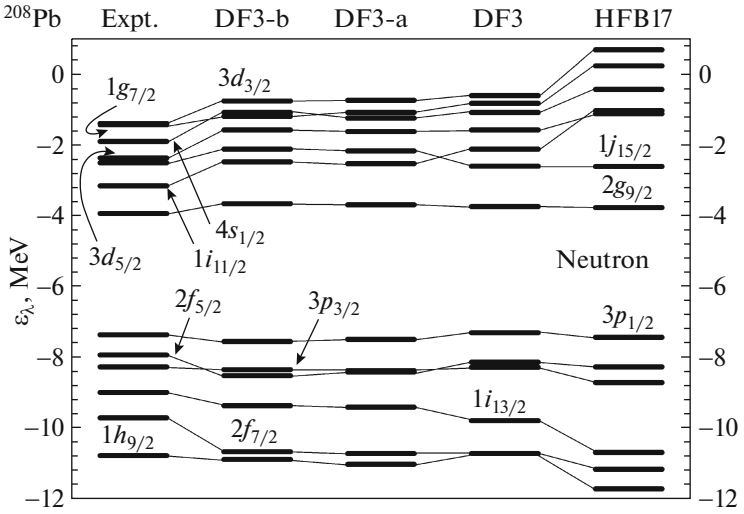

Fig. 2. Neutron single-particle levels in ^{208}Pb. The experimental data on display were borrowed from [22].

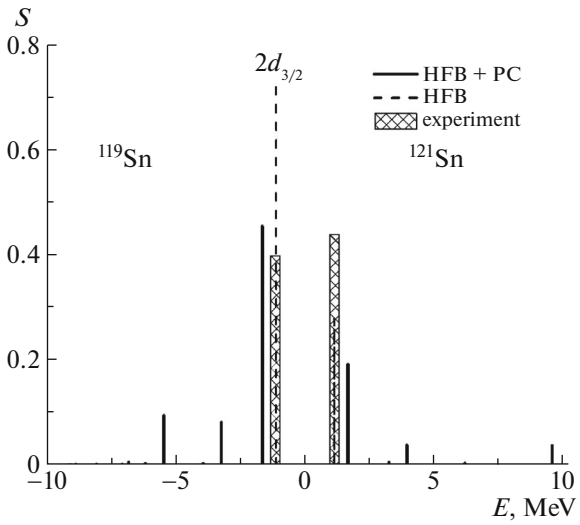

Fig. 3. Spectroscopic factors (single-particle strength) calculated for the $d_{3/2}$ orbital in ^{119}Sn and ^{121}Sn. The experimental data on display were borrowed from [23–25].

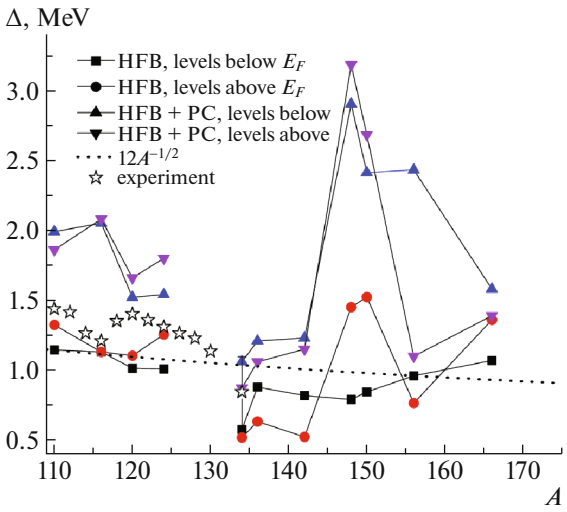

Fig. 4. Neutron gap with allowance for quasiparticle–phonon interaction in tin isotopes (results of calculations with SLy4 Skyrme forces) [26].

quasiparticle–phonon model [2, 44] (for more details, see references in [45]).

A new effect of three-quasiparticle ground-state correlations (GSC), which proved to be large [in contrast to two-quasiparticle GSC appearing in the quasiparticle random-phase approximation (QRPA)] and which saturate one-half of anharmonic corrections, was first considered in [45]. It should be noted that, in the g^2 approximation, these new GSC were in fact taken into account within the NFT framework [46] and within the Green's function method [47], but they were not singled out quantitatively and were not specially called.

The study reported in [11] and performed for magic nuclei on the basis of the Green's function method and within the TFFS framework [12] played an important role in exploring second- and third-order effects. In that study, the condition of consistency between the mean field and nuclear interaction was used, which permitted avoiding the introduction of new parameters. As a starting point, use was made there of RPA—more precisely, the Bohr–Mottelson approximation—in order to calculate the amplitude g with allowance for all g^2 corrections. For the g^2 problem, the inclusion of these corrections is accomplished by introducing phonon-tadpole effects (see Fig. 1), which should be taken into account in the corrections to the mean field (for more details, see [6]). The quantity $\delta_1 g_2$, which appears in the definition

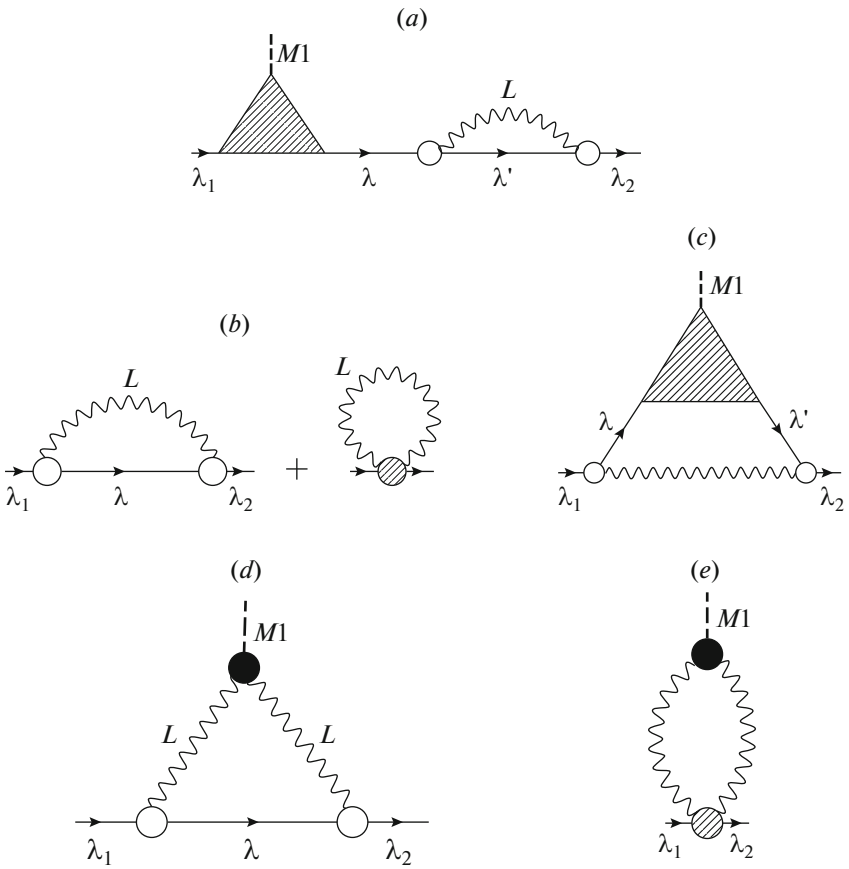

Fig. 5. Corrections for quasiparticle–phonon interaction to static electromagnetic moments: (*a*) "end" corrections for quasiparticle–phonon interaction, (*b*) corrections for quasiparticle–phonon interaction to the mass operator, (*c*) interaction-induced corrections for quasiparticle–phonon interaction, (*d*) corrections induced by the direct action of the electromagnetic field on the phonon, and (*e*) tadpole-like diagram for the contribution of the phonon electromagnetic field.

of the tadpole, satisfies the integral equation (4) and takes into account all g^2 terms.

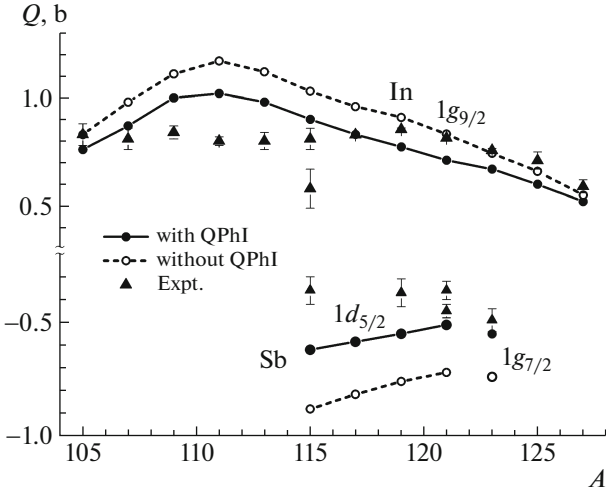

Fig. 6. Ground-state quadrupole moments of odd indium and antimony isotopes after and before taking into account corrections for quasiparticle–phonon interaction. The experimental data on display were taken from [37].

According to [11], the amplitude of the transition for two phonons under the effect of the external field V_0 has the form

$$M^{(2)} = V_0GGg_1Gg_2 + V_0GGg_{12}, \qquad (13)$$

where g_{12} can be represented in the form of the diagrams in Fig. 7. Hereafter, g is treated within the RPA—more precisely, TFFS—framework. After some algebra, the expression for $M^{(2)}$ can be represented in the form

$$M^{(2)} = VGGGg_1g_2 + VGG\delta_1FGGg_2; \qquad (14)$$

that is, the final expression for $M^{(2)}$ contains the nuclear-polarizability effect described in RPA (more precisely, TFFS) terms (first term) and δF (second term). The calculations performed in [45] show that the contribution of this, second, term is small.

For nuclei with pairing, it is also necessary to make use of the anomalous Green's functions $F^{(1)}$ and $F^{(2)}$ and six additional diagrams, some of which are shown in Fig. 8. In the case of identical phonons, the final expression for the amplitude $M^{(2)}$ (phonon

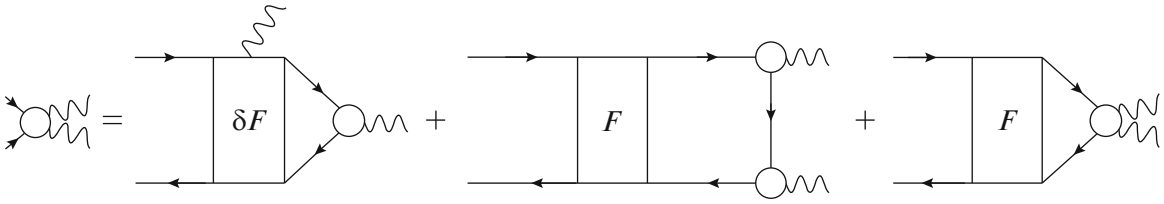

Fig. 7. Equation (4) in a diagram form.

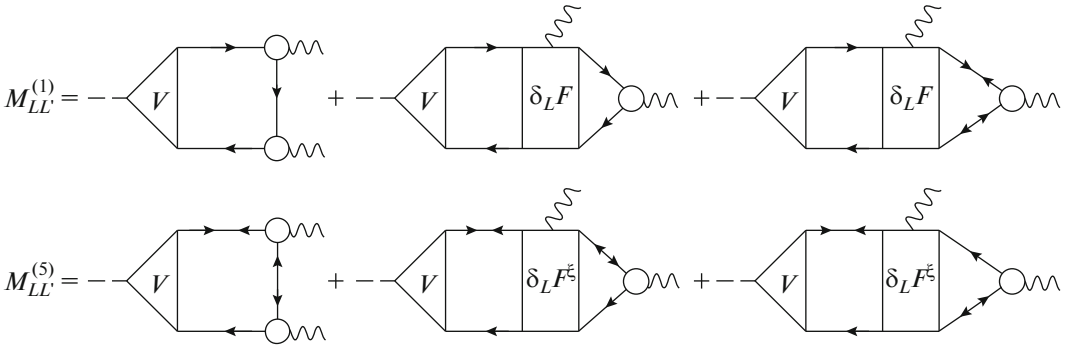

Fig. 8. Matrix elements $M^{(1)}$ and $M^{(2)}$ for nuclei where pairing is present.

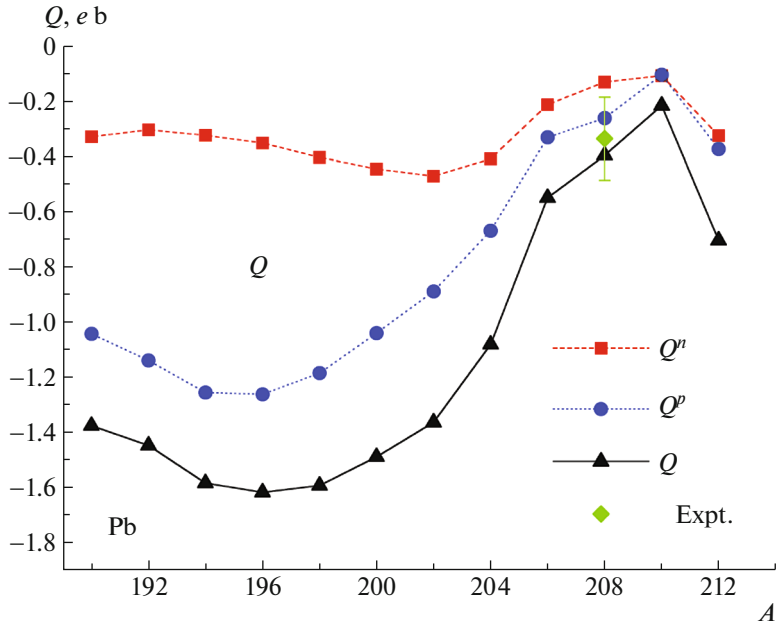

Fig. 9. Quadrupole moments of the first 3^- states in even lead isotopes.

static moment) has the form

$$M^{(2)}_{LL} = \sum_{123}(-1)^{L+1}\begin{pmatrix} I & L & L \\ 0 & L & -L \end{pmatrix}\begin{Bmatrix} I & L & L \\ j_3 & j_2 & j_1 \end{Bmatrix} \times \langle 1 \parallel V \parallel 2\rangle\langle 3 \parallel g_L \parallel 1\rangle\langle 2 \parallel g_L \parallel 3\rangle \sum_{i=1}^{8} A^{(i)\text{pair}}_{123}, \quad (15)$$

where

$$\sum_{i=1}^{8} A^{(i)\text{pair}}_{123} = \left(\frac{1}{(\omega_L + E_{13})(\omega_L + E_{23})} + \frac{1}{(\omega_L - E_{13})(\omega_L - E_{23})}\right) \times \left[u_1^2 u_2^2 v_3^2 - v_1^2 v_2^2 u_3^2 + \frac{\Delta_1\Delta_2}{4E_1E_2}(u_3^2 - v_3^2)\right. \quad (16)$$

Table 4. Transition probabilities $B(EL)\downarrow$ e^2 fm^{2L} (the quoted experimental data were taken from [21]; in column 4, the results of the calculations are given without taking into account new GSC and the nuclear polarizability; the values in column 5 were obtained with GSC $\neq 0$ and with the polarizability estimated in terms of e_{eff}; in column 6, the results are presented for GSC $= 0$ and upon taking into account the polarizability via solving Eq. (2) for the vertex; and final results are given in column 7)

1	2	3	4	5	6	7	8
EL	Transition	Nucleus	GSC $= 0$ $V = e_q V_0$	GSC $\neq 0$ $e_{\text{eff}} \neq 0$	GSC $= 0$ $V \neq 0$	GSC $\neq 0$ $V \neq 0$	Expt.
$E1\downarrow$	$3^-_1 \to 2^+_1$	^{132}Sn	7.6×10^{-4}	2.8×10^{-2}	6.9×10^{-5}	1.3×10^{-3}	$>2.8 \times 10^{-4}$
	$2^+_1 \to 3^-_1$	^{208}Pb	2.45×10^{-4}	8.19×10^{-4}	2.4×10^{-5}	9.5×10^{-4}	$(7.9 \pm 2.7) \times 10^{-4}$
$E2\downarrow$	$5^-_1 \to 3^-_1$	^{132}Sn	3.28×10^{-3}	7.79	13.8	25.7	24.3 ± 1.2
	$5^-_1 \to 3^-_1$	^{208}Pb	19.35	36.21	46.0	18.8	27.9 ± 1.5

$$+\frac{\Delta_1\Delta_3}{4E_1E_3}(u_2^2-v_2^2)+\frac{\Delta_2\Delta_3}{4E_2E_3}(u_1^2-v_1^2)\Bigg]$$
$$+\frac{1}{E_{12}}\Bigg[\frac{2E_{23}(u_1^2u_3^2v_2^2-v_1^2v_3^2u_2^2)}{E_{23}^2-\omega_L^2}$$
$$+\frac{2E_{13}(u_2^2u_3^2v_1^2-v_3^2v_2^2u_1^2)}{E_{13}^2-\omega_L^2}$$
$$-\left(\frac{\Delta_1\Delta_2}{2E_1E_2}(u_3^2-v_3^2)+\frac{\Delta_1\Delta_3}{2E_1E_3}(u_2^2-v_2^2)\right.$$
$$\left.+\frac{\Delta_2\Delta_3}{2E_2E_3}(u_1^2-v_1^2)\right)\left(\frac{E_{13}}{E_{13}^2-\omega_L^2}+\frac{E_{23}}{E_{23}^2-\omega_L^2}\right)\Bigg].$$

Here, $E_{12}=E_1+E_2$, $E_1=\sqrt{(\varepsilon_1-\mu)^2+\Delta_1^2}$, and the subscripts $1\equiv(n_1,l_1,j_1)$ (spherical nuclei) denote sets of single-particle quantum numbers. Further, V and g_L are, respectively, the effective field that determines the nuclear polarizability and the amplitude for the production of a photon characterized by an angular momentum L and an energy ω_s. These quantities are determined by the TFFS equations (2) and (3) in which it is necessary to take pairing into account [12]. The second half of expression (16), which involves the factor $(E_{12})^{-1}$, describes new (that is, three-quasiparticle) GSC.

Figure 9 shows the quadrupole moments in the first 3^- state that were obtained from a self-consistent calculation for lead isotopes with the DF3-a Fayans functional. In our calculations, the value of $Q(3^-_1)$ is determined by two effects: the GSC effect (which is responsible for 50% to 60% of Q_{tot}) and the nuclear polarizability (which saturates approximately 40% to 50% of Q_{tot}). These two effects have identical signs, in contrast to what we have in the case of $E1$ transitions in the doubly magic nuclei ^{132}Sn and ^{208}Pb (see below), where they compensate strongly each other. For ^{208}Pb, in which case there is only one experimental value of $Q(3^-_1)=-0.35\pm0.15$ e b, we obtained $Q(3^-_1)=-0.40$ e b. In this value, the GCS contribution is $[-0.40-(-0.18)]=-0.22$ e b (55%), while the polarizability contribution is $[-0.18-(-0.074)]=-0.17$ e b (43%). In the final result, Q_{tot}, all values of the proton and neutron components are negative. The values calculated for $Q(3^-_1)$ in semimagic nuclei exceed $Q(3^-_1)$ in the magic nucleus of ^{208}Pb by a factor of two to three for all lead isotopes, with the exception of ^{210}Pb and ^{206}Pb, and by a factor of three to four for all tin isotopes, with the exception of ^{102}Sn. This complies with the qualitative assumptions on the values of $Q(3^-_1)$ in [1] (p. 501), even though there is no order-of-magnitude distinction for semimagic nuclei studied thus far.

Table 4 gives the results obtained for another second-order effect—the probabilities for $E1$ and $E2$ transitions in the doubly magic nuclei ^{208}Pb and ^{132}Sn—from self-consistent calculations performed with the DF3-a Fayans functional. Good agreement with experimental data were obtained. In order to estimate the role of individual effects that determine $B(EL)$, the results of various approximate calculations are presented in columns 4, 5 and 6. The polarization effects for $E1$ transitions are determined first of all by the difference in sign between the local charges $e_q^p(E1)$ and $e_q^n(E1)$. However, the inclusion of GSC increases $B(E1)$ by more than one order of magnitude (columns 6 and 7), whereas the inclusion of the polarizability reduces this quantity by one order of magnitude as well (see columns 4 and 6); that is, the final result for the observed effect is the difference of two large values. This highlights the importance of self-consistency in the computational scheme used. For $E2$ transitions, the inclusion of GSC changes $B(E2)$ values by a factor of two to three, while the inclusion of the polarizability increases the effect

differently for different nuclei. More detailed results can be found in [45, 48–50].

2.3. Third-Order Anharmonic Effects

The amplitude of the transition *for three phonons* under the effect of the external field V_0 has the form [11]

$$M^{(3)} = V_0GGg_1Gg_2Gg_3 + V_0GGg_{12}Gg_3 + V_0GGg_{123}. \quad (17)$$

In order to derive, for $M^{(3)}$, an expression that similar to Eq. (13) for $M^{(2)}$, it is necessary to obtain a more complicated integral equation for g_{123} by varying Eq. (4); that is,

$$g_{123} = \delta_1\delta_2FGGg_3 + \delta_1FGg_2Gg_3G + \delta_1FGGg_{12} + FGg_{12}Gg_3G + FGg_1Gg_2Gg_3G + FGGg_{123}. \quad (18)$$

This equation (Fig. 10) contains five [rather than two as g_{12} in (4)] various free terms, apart from similar terms arising from phonon permutations. Replicating, by analogy, the derivation of $M^{(2)}$, we obtain an expression for $M^{(3)}$ in the form

$$M^{(3)} = VGg_1Gg_2Gg_3G + VGg_{12}Gg_3G + VGG\delta_1FGGg_{12} + VGG\delta_1FGg_1Gg_2G + VG\delta_1\delta_2FGg_3G. \quad (19)$$

In terms of Feynman diagrams, it can be represented in the form shown in Fig. 11.

By analogy with the results obtained in [45] on the smallness of the diagrams involving δF, we can assume that the diagrams in Fig. 11 that contain δF and $\delta_1\delta_2F$ also make a small contribution. The diagram in Fig. 11 with g_{12} determines the effects of the phonon tadpole. As far as we know, it has never attracted the attention of theorists. In the following, we therefore consider, for the problem of interaction of three phonons, only the first diagram in Fig. 11 with four Green's functions. For the problem involving three "equivalent" phonons that was considered in [11], it is necessary to take into account phonon permutations, so that, in fact, we should evaluate the contribution of six such diagrams.

In order to consider nuclei with pairing in terms of Green's functions, it is necessary to make use of four Green's functions: G, G^h, $F^{(1)}$, and $F^{(2)}$ [12]. Following the above line of reasoning in the problem with pairing [45], we spell out the first diagram for $M^{(3)}$ with allowance for these Green's functions. In doing this, we take into account, as in [45], only particle–hole (ph) vertices. We disregard particle–particle (pp) and hole–hole (hh) vertices, since they usually make a small contribution and since their inclusion would complicate the problem being considered substantially. In the case of pairing, it is then necessary to calculate the contribution of seven types of diagrams containing the products $F_1^{(1)}F_2^{(2)}$.

It is of interest to consider the specific case of a transition between a two-phonon and a one-phonon state in nuclei with pairing, since, for this case, there are experimental data and calculations based on different models. The problem of the $E1$ transition between a specific two-phonon and a specific one-phonon state in nuclei with pairing was considered in [44]. The authors of [44] calculated the probability for the observed $E1$ transitions from the two-phonon 1^- state consisting of low-lying first one-phonon 2^+ and 3^- states to the one-phonon 2^+ state in three nuclei (Sn, Sm, and Nd) and reached good agreement with experimental data. By analogy with [44], we have considered the $[1 \times 2] \to 4$ transition between the two-phonon state and the 4 one-phonon state.

The results obtained in [44] arise within the approach considered here if, in particular, we neglect the following terms in the integral of four Green's functions that contains 14 terms involving the product of four Bogolyubov coefficients:

(i) four-quasiparticle GSC—that is, four terms of the $u^2u^2v^2v^2$ type, where u^2 and v^2 are the Bogolyubov coefficients squared, which appear in the definition of Green's functions in nuclei with pairing [12];

(ii) eight terms of the $u^2v^2v^2v^2$ or $u^2u^2u^2v^2$ type, which are possibly four-quasiparticle GSC as well;

(iii) δ_1g_2 diagrams (second ones in Fig. 11), which contain tadpole effects and three-quasiparticle GSC;

(iv) Terms in Fig. 11 with δF and $\delta_1\delta_2F$, which are likely to be small.

Since the authors of [44] obtained a good description of experimental data, we cannot rule out the possibility that future complicated calculations will show that all of the disregarded effects compensate for one another.

3. PYGMY DIPOLE AND GIANT DIPOLE RESONANCES

We now consider the region of PDR and GDR energies, which is a different region of nuclear excitations and where one employs Skyrme functionals and takes into account coupling to phonons within the method of quasiparticle time-blocking approximation (QTBA) for magic and semimagic nuclei [16, 15, 18]. The most recent method of continuum time-blocking approximation (CTBA) (see Subsection 3.4) is also used for magic nuclei.

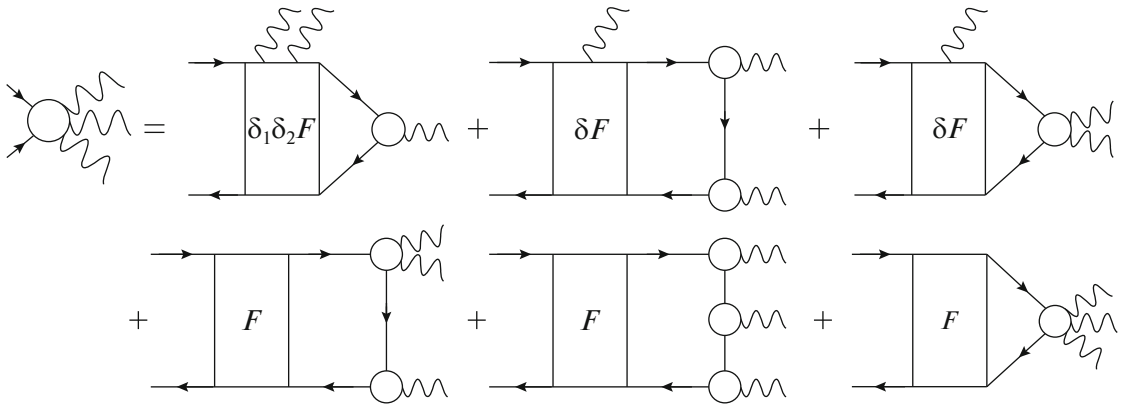

Fig. 10. Equation (18) in a diagram form.

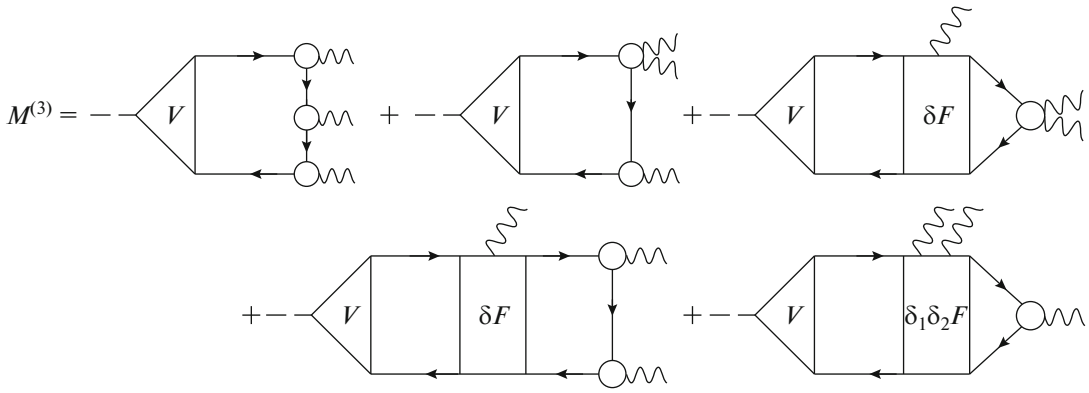

Fig. 11. Equation (19) in a diagram form.

The concept of the radiative strength function (RSF) $f_{E1}(\omega)$ is a key point here. Under the assumption that the Brink–Axel hypothesis is valid, this concept is used to describe radiative nuclear reactions in terms of

$$f_{E1}(\omega) = \frac{1}{3(\pi\hbar c)^2}\frac{\sigma_{\rm abs}(\omega)}{\omega}, \qquad (20)$$

where ω is the gamma-ray energy and $\sigma_{\rm abs}$ is the photoabsorption cross section.

3.1. Contribution of Quasiparticle–Phonon Interaction to Radiative Strength Functions

In Figs. 12 and 13, the radiative strength functions in the PDR region for tin and nickel isotopes are given along with their experimental counterparts obtained by means of the "Oslo method" [51–54] and on the basis of the popular EGLO (Enhanced Generalized LOrentzian) phenomenological model. These figures show that, in contrast to what we have within the EGLO phenomenological model, the pygmy dipole resonance in tin and nickel isotopes develops a structure caused both by effects of the self-consistent method of the quasiparticle random-phase approximation (QRPA) and by effects of coupling to phonons. The structures associated with the effects of coupling to phonons arise in the calculations because of the existence of poles at the energies $E = E_1 + E_2 - \omega_s$, where $E_{1,2}$ and ω_s are, respectively, the quasiparticle and phonon energies. In the PDR region, the effects of coupling to phonons are sizable at energies between 3 MeV and 9 to 10 MeV.

Further, a good microscopic description of experimental data in the PDR region [51–54] is attained only owing to taking into account effects of coupling to phonons. However, the enhancement observed for the ^{70}Ni nucleus in the energy region of $E_\gamma < 3$ MeV is similar to the enhancement found in the strength function for ^{94,96}Mo nuclei [55] and explained by nucleon $E1$ transitions from single-particle states to a single-particle continuum [56] or $M1$ transitions between excited states because of spin reorientation in proton and neutron states characterized by high values of j [57].

For the ^{68}Ni nucleus, which is neutron-rich and which has the neutron separation energy of $S_n = 7.79$ MeV, Wieland and his coauthors [58] measured

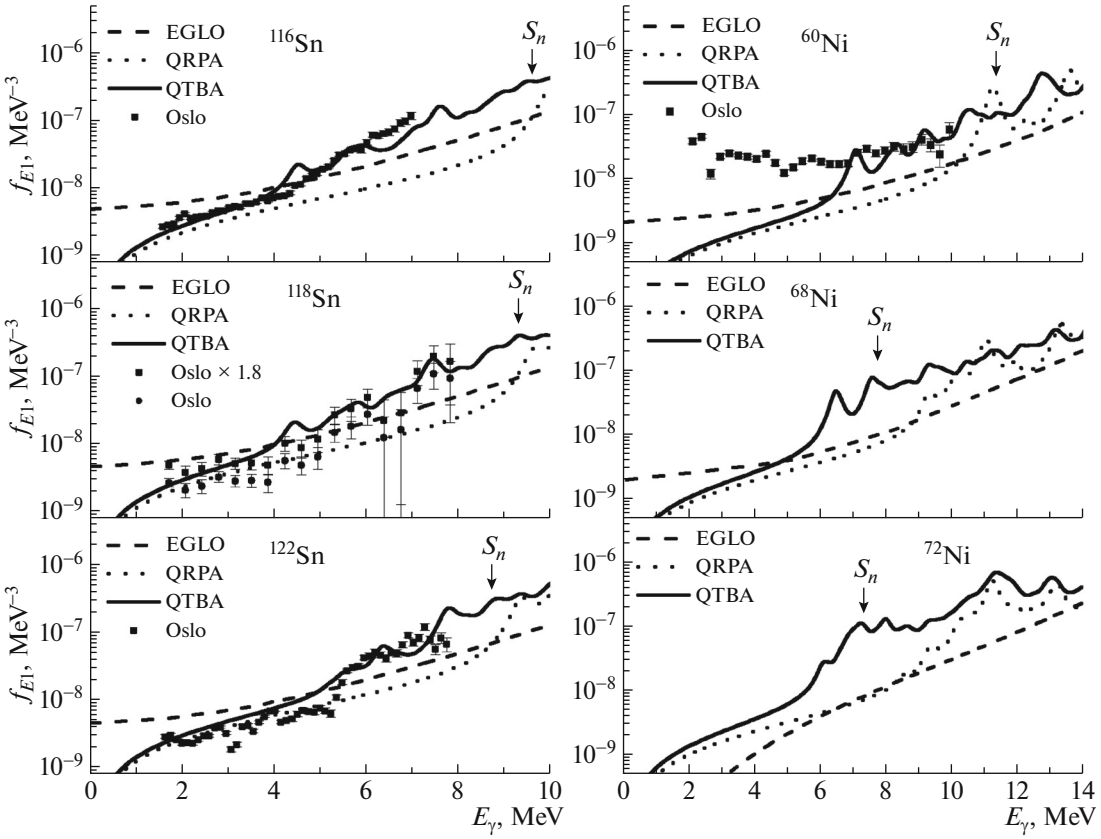

Fig. 12. Radiative strength function for the isotopes ^{116,118,122}Sn and ^{60,68,72}Ni. The results of calculations based on the EGLO phenomenological model, microscopic calculations within the QRPA framework, and calculations within the self-consistent version of generalized TFFS (QTBA) are represented by, respectively, the dashed, dotted, and solid curves. The experimental data on display were borrowed from [51] for tin isotopes and from [52] for the ^{60}Ni nucleus.

features of the PDR and obtained the following results: the PDR lies in the range between 7 and 13 MeV, having a mean energy of about 11 MeV, and exhausts approximately 5% of the energy-weighted sum rule; that is, the PDR is well above the neutron separation energy. In the interval of observation between 7 and 13 MeV, good agreement with experimental data on the mean PDR energy ($\langle E\rangle =$ 11.2 MeV) and a satisfactory description of the exhaustion of the sum rule (4.85%) were obtained by our group on the basis of QRPA calculations. Upon taking into account coupling to phonons, the mean energy undergoes virtually no change, becoming $\langle E\rangle =$ 10.9 MeV, but the degree of exhaustion (in percent) of the sum rule grows substantially, to 8.7%. Earlier, the authors of [56, 59] performed similar calculations for ^{68}Ni and ^{70}Ni within the relativistic version of QTBA, but they had to take additionally into account two-phonon configurations in order to explain experimental data.

Figure 13 shows that, for the ^{70}Ni nucleus ($S_n =$ 7.31 MeV), the radiative strength function obtained on the basis of the EGLO model does not have structures up to an energy of 14.5 MeV; on the contrary, a microscopic approach yields distinct structures for $E > S_n$ both within the QRPA and within the QTBA framework. Thus, we have obtained $\langle E\rangle = 12.2$ MeV for the interval between 8 and 14 MeV and $\langle E\rangle =$ 11.4 MeV for the interval between 7.3 and 13.3 MeV. With allowance for coupling to phonons, the degree of exhaustion of the energy-weighted sum rule is 20.6% and 27.7% in the cases of, respectively, QRPA and QTBA calculations in the first interval and 12.7% and 19.5% for the same approximations in the second interval. Thus, the quantitative effect of coupling to phonons in terms of the difference between the QRPA and QTBA results is the strongest for the degree of exhaustion of the energy-weighted sum rule. The mean values $\langle E\rangle$ remain nearly unchangeable for all three versions (QRPA, QTBA, and EGLO). The results of our calculations for the ^{70}Ni nucleus in the PDR region (more precisely, in the energy range between 5 and 9 MeV) were already confirmed by the most recent experimental data [53, 54].

For the features of the PDR in the ^{72}Ni nucleus ($S_n = 6.89$ MeV) in the energy range between 8 and 14 MeV, it was found within the QTBA framework

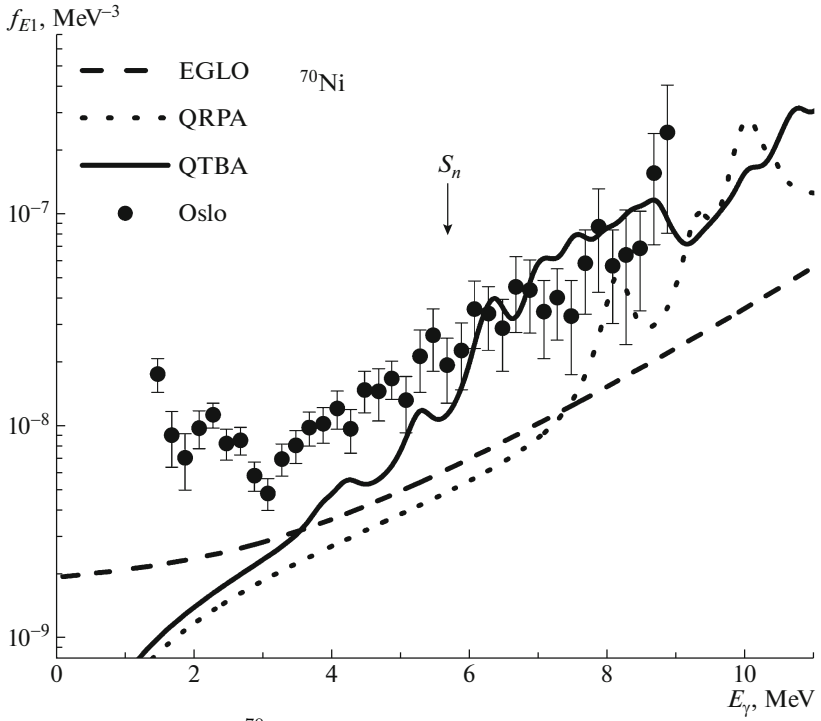

Fig. 13. As in Fig. 12, but for ^{70}Ni. The experimental data on display were taken from [53, 54].

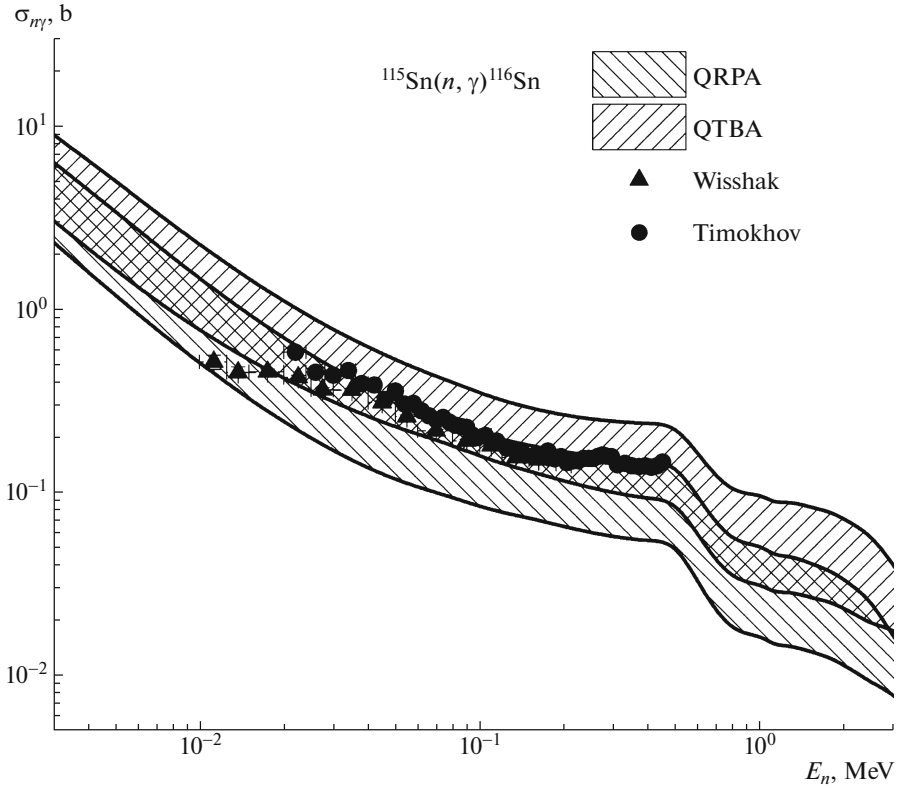

Fig. 14. Cross sections for radiative neutron capture according to calculations based on the QRPA and QTBA methods. The uncertainty band is associated with employing different models for the nuclear level density. The experimental data on display were taken from [67, 68].

that the mean energy is $\langle E \rangle = 12.4$ MeV and that the PDR exhausts 25.7% of the energy-weighted sum rule. So large a value of the degree of sum-rule exhaustion is due to the fact that the nucleus in question is a highly neutron-rich nucleus. It is noteworthy that a dominant contribution to the PDR in ^{72}Ni lies

Table 5. Average radiative widths Γ_γ (in meV units) for s-wave neutrons {for each of the adopted approaches (EGLO, QRPA, and QTBA), use was made of two models for the nuclear level density: the phenomenological generalized superfluid model (GSM) [71] (first row) and the microscopic combinatorial plus Hartree–Fock–Bogolyubov (HFB) model [72] (second row)}

	^{110}Sn	^{112}Sn	^{116}Sn	^{118}Sn	^{120}Sn	^{122}Sn	^{124}Sn	^{58}Ni	^{60}Ni	^{62}Ni	^{68}Ni	^{72}Ni
EGLO	147.4	105.5	72.9	46.6	55.0	56.6	49.9	1096	474	794	166	134
	207.9	160.3	108.9	106.7	124.3	110.2	128.7	2017	1882	1841	982.2	86.4
QRPA	45.6	34.4	30.4	22.1	23.8	27.9	22.3	358	594	623	75.4	83.8
	71.0	49.7	44.3	40.3	43.0	50.1	68.9	450.8	1646	490.9	406.4	46.7
QTBA	93.5	65.7	46.8	33.1	34.1	35.8	27.9	1141	971	1370	392	154
	119.9	87.0	58.4	58.1	61.5	64.0	84.8	1264	2800	2117	2330	53.8
Expt. [78]	–	–	–	117 (20)	100 (16)	–	–	–	2200 (700)	2000 (300)	–	–
[71]	–	–	–	80 (20)	–	–	–	–		2200 (700)	–	–
Syst.	112	109	107	106	105	104	103	2650	1900	1300	420	320

in the energy range between 10 and 14 MeV and saturates 13.9% (within the QRPA framework) or 23.2% (within the QTBA framework) of the energy-weighted sum rule; that is, the effect of coupling to phonons is quite significant. There are two maxima in this energy range (see Fig. 12). For this reason, the radiative strength function in the range between 10 and 14 MeV is nearly coincident with that in the range between 8 and 14 MeV.

More detailed results on the subject can be found in [60–66].

3.2. Radiative Neutron Capture

Figure 14 shows radiative neutron capture cross sections obtained for some tin isotopes by means of the EMPIRE code [69] with the radiative strength functions that we calculated on the basis of microscopic methods. The calculations were performed by employing several models for the nuclear level density, such as the enhanced generalized superfluid model (EGSM) [70], the generalized superfluid model (GSM) [71], and the microscopic combinatorial plus Hartree–Fock–Bogolyubov (HFB) model [72]. The cross sections for radiative neutron capture in nuclei for which there are no experimental data were calculated on the basis of the EGLO phenomenological model of the radiative strength function and the combinatorial plus HFB model of the nuclear level density. One can see from Fig. 14 that the QRPA method underestimates the cross sections in question, and only upon taking into account coupling to phonons is it possible to describe experimental data microscopically, irrespective of the choice of model for the nuclear level density. Such an underestimation of the cross sections is usually remedied by an empirical shift and a broadening of the strength distribution within the QRPA framework to the region of low energies [5, 73]. For more detailed results, the interested reader is referred to [74–77].

3.3. Average Radiative Widths of Neutron Resonances

The average radiative widths of neutron resonances, Γ_γ, are an important feature of gamma decay from highly excited states. They are required in calculations for nuclear reactions and are given by

$$\Gamma_\gamma = \sum_{I=|J-1|}^{J+1} \int_0^{S_n} \epsilon_\gamma^3 f_{E1}(\epsilon_\gamma) \frac{\rho(S_n - \epsilon_\gamma, I)}{\rho(S_n, J)} d\epsilon_\gamma, \quad (21)$$

where ρ is the level density in excited nuclei and J is the spin of the original compound nucleus.

Table 5 gives the Γ_γ values calculated for seven semimagic tin isotopes and five semimagic nickel isotopes by means of the EMPIRE code [69] for three different models of the radiative strength function—the EGLO phenomenological model and the QRPA and QTBA microscopic models—that are combined with various models of the nuclear level density, such as GSM [71] and the microscopic combinatorial plus HFB model [72]. The calculated widths are compared with experimental data [78], if any, and with existing systematics [70, 71]. Table 5 shows that, for stable nuclei, the inclusion of the effects of coupling to phonons improves substantially agreement with the systematics, especially with respect to the QRPA results. Coupling to phonons leads to an increase of 50 to 200% in the Γ_γ values for all of the isotopes,

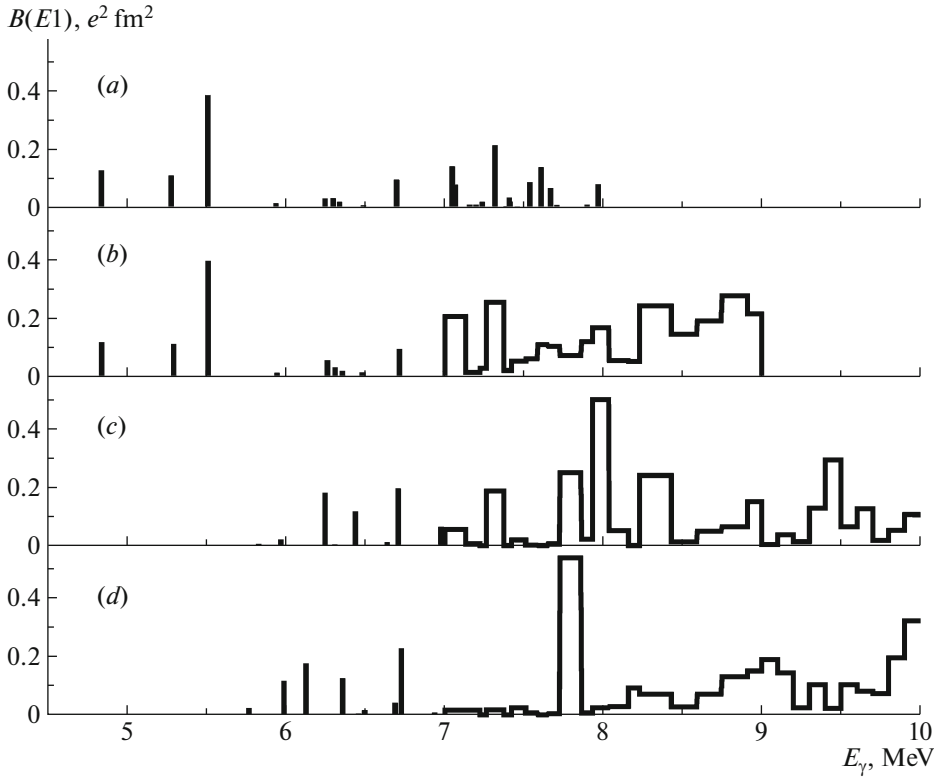

Fig. 15. Experimental and theoretical spectrum of $E1$ excitations in ^{208}Pb in the PDR region: (*a* and *b*) experimental data from [85] and [81], respectively, and (*c* and *d*) results obtained with the CTBA framework with, respectively, SV-bas$_0$ and SV-bas$_1$.

with the exception of ^{122}Sn and ^{124}Sn, where the respective increase is moderately small.

The results for Γ_γ in ^{118}Sn, ^{120}Sn, ^{60}Ni, and ^{62}Ni, for which there are experimental data, are the most interesting. Good agreement with experimental data for ^{60}Ni and ^{62}Ni and reasonable agreement for ^{118}Sn and ^{120}Sn were obtained on the basis of QTBA and the microscopic combinatorial plus HFB model of the nuclear level density [72]. It should be noted that the $M1$-resonance contribution calculated according to the recommendation from [71] is taken into account in evaluating the width Γ_γ. In determining the contribution of the $M1$ resonance to Γ_γ, use is made of a standard Lorentz parametrization [71] with a width of $\Gamma = 4$ MeV [1] (this value of the width Γ can be questioned, as was discussed in [79]). It turned out that this contribution is about 10% to 12% of the values in the first row of Table 5 for tin isotopes and 4%, 3%, 22%, and 16% for ^{58}Ni, ^{62}Ni, ^{68}Ni, and ^{72}Ni, respectively. In our opinion, the problem of the $M1$-resonance contribution to Γ_γ deserves a special analysis.

Agreement of the values calculated for Γ_γ with experimental data becomes poorer upon employing the EGLO or QRPA model, as well as GSM for the model of the nuclear level density. For stable nuclei, the results of the combinatorial plus HFB model are in better agreement with the systematics in [70] than the GSM-based results. Similar conclusions can also be drawn for the EGLO model.

More detailed results can be found in [77, 80].

3.4. The Most Recent Theory of the PDR and GDR. Fine Structure of the PDR in ^{208}Pb

In describing the PDR in ^{208}Pb, the main problem arising within self-consistent models consists in the deficiency of the $E1$ strength at excitation energies below 6 MeV, where, in experiments, one observes about 30% of the integrated PDR strength (see [81]). The question of whether it is possible to describe the PDR and GDR simultaneously within a single model is yet another challenge in view of the fact that the shape of the GDR strength function in RPA differs strongly in the majority of cases from the experimental distribution. Therefore, the problem of describing integrated features of the PDR in ^{208}Pb and its fine structure has still remained open.

It would therefore be reasonable to calculate $E1$ excitations in the energy region of the PDR in the ^{208}Pb nucleus on the basis of the fully self-consistent CTBA method [82, 83], which was recently developed for nuclei without pairing and in which a single-particle continuum is fully taken into account at the

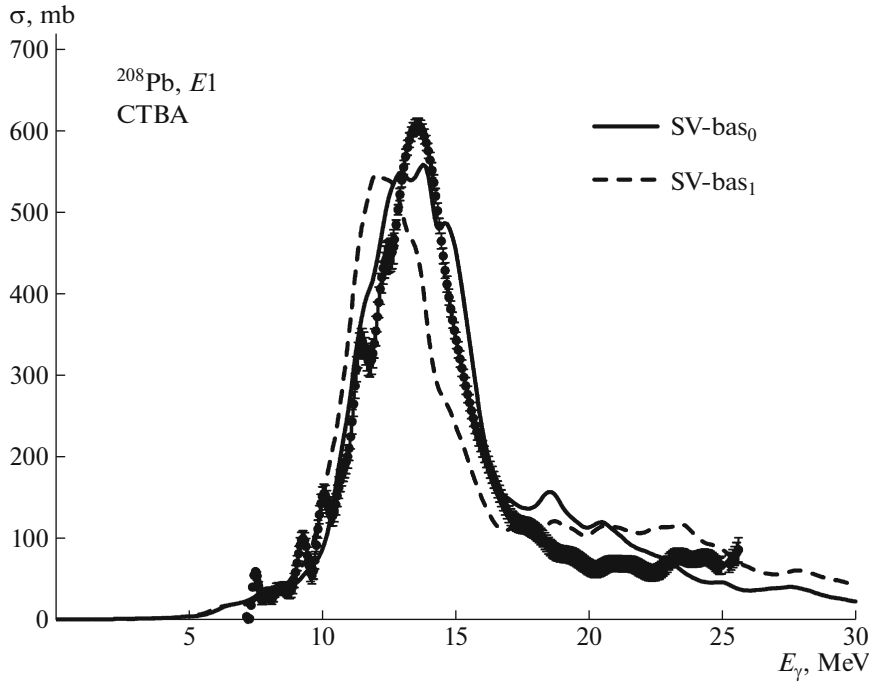

Fig. 16. Photoabsorption cross section calculated for ^{208}Pb by the CTBA method with (solid curves) SV-bas$_0$ and (dashed curve) SV-bas$_1$ Skyrme forces. The energy smoothing parameter was set to the value of $\Delta = 400$ keV. The points on display represent experimental data from [89].

RPA level in addition to effects of quasiparticle–phonon interaction. This method was earlier applied in [66] in order to explain the experimental results obtained by the "Oslo method" in [84] for the radiative strength function in ^{208}Pb. In accordance with the experimental data, the smoothing parameter value of $\Delta = 200$ keV was used in the calculations, and quite a reasonable description of experimental data from [84] for the $E1$ radiative strength function in the range between 5 and 7.5 MeV was obtained. In contrast to what was done in [66], all 1^- levels of ^{208}Pb and strength functions for $E1$ excitations in this nucleus for energies between 0 and 10 MeV are presented in Fig. 15 according to calculations with the smoothing parameter values of $\Delta = 1$ and 10 keV.

It is also of interest to study the effect of so-called residual spin–spin forces (RSSF) on the properties of low-lying 1^- levels. These forces are taken into account self-consistently and without the introduction of new parameters.

In Fig. 15, the results obtained by calculating the fine structure of the PDR in ^{208}Pb are shown along with experimental data. Figures 15*a* and Fig. 15*b* give experimental data from [85] and [81], respectively. Those experiments involved measuring the reduced probabilities $B(E1)$ for excitations up to the neutron separation energy and the sums of the probabilities for respective energy intervals above this threshold. Figures 15*c* and 15*d* give the results obtained by the CTBA method for, respectively, SV-bas$_0$ and SV-bas$_1$ forces with or without RSSF. The analysis of experimental data in [81] reveals that the PDR in ^{208}Pb lies in the energy region below 8.23 MeV.

The data presented in [81, 85, 86] also show that the PDR in this nucleus can be broken down into two broad resonances: the lower PDR (LPDR—in the energy range extending from 4.8 to approximately 5.7 MeV) and the higher PDR (HPDR—in the energy range extending from 5.7 to 8.23 MeV). Above 8.23 MeV, the UPDR borders on the low-energy GDR tail. We note that the UPDR lies in the region of the so-called $1\hbar\omega$ isoscalar dipole resonance (see [87, 88]), whose energy calculated on the basis of the harmonic-oscillator shell model is 6.9 MeV in ^{208}Pb. Our research of the effect of residual spin–spin forces on the properties of low-lying 1^- levels reveals that this effect may be sizable, but only upon refining the respective parameters of the Skyrme energy density functional, which have still remained poorly known, can we draw a definitive conclusion on the point under discussion.

The $E1$-excitation strengths calculated by the CTBA method over a broad (0–30 MeV) energy interval by employing two force parametrizations (SV-bas$_0$ and SV-bas$_1$) and the smoothing parameter of $\Delta = 400$ keV are given in Fig. 16. A sizable downward shift of the distributions obtained with the SV-bas$_1$ parametrization is explained primarily

by a large difference in the number of phonons in the CTBA phonon basis constructed according to the new criterion of collectivity (see [90, 91]): 28 phonons in the case of SV-bas$_0$ and 83 phonons in the case of SV-bas$_1$. Calculations show that, within this approach, one can simultaneously obtain a good description of the GDR structure in ^{208}Pb and integrated properties of the PDR in the energy region above 5.7 MeV. A theoretical description of the PDR below this energy within a self-consistent model requires a further development of the theory, including searches for new parametrizations of the Skyrme energy density functional or, possibly, searches for new functionals. More detailed results on this subject can be found in [82, 83, 90–100].

4. CONCLUSIONS

We have considered the contribution of quasiparticle–phonon interaction to the characteristics of nuclei and nuclear reactions involving gamma rays over a broad energy region—from the ground state to the energies of pygmy and giant dipole resonances. We have shown that, as a rule, the inclusion of coupling to phonons is mandatory for explaining experimental data. This coupling generates additional structures in radiative strength functions and, as a matter of fact, is at odds with the Lorentzian approximation usually used in nuclear reaction theory. A self-consistent inclusion of quasiparticle–phonon interaction makes it possible to predict reliably a large number of nuclear features. An analysis of quasiparticle–phonon interaction within nuclear quantum many-body theory permits considering new effects—first of all, three- and four-quasiparticle ground-state correlations. Third-order anharmonic effects within nuclear many-body theory are of particular interest since they contain radically new effects and allow one to test the well-known Brink–Axel hypothesis.

In the two energy regions being considered, we have employed a unified approach that relies on the Green's function formalism and which is a natural development of the theory of finite Fermi systems toward consistently taking into account quasiparticle–phonon interaction. This unified approach connects the two energy regions in question and gives grounds to hope for merging them together within the future version of a "unified" theory. In this connection, it would be of use to list some problems as-yet-unresolved within the self-consistent microscopic approach for the two energy regions. Specifically, we mean, for nuclei without pairing, the problem of consistently taking into account tadpole effects for the PDR and GDR regions (our group made the first step along this line in [18]); for nuclei with pairing, the problem of taking into account pairing-tadpole effects [27] in the two energy regions; the problem of taking into account configurations more complex than the $1p1h\otimes$phonon configuration {this is necessary first of all for the theory of the PDR and GDR, but advances made here within the Green's function method are quite slow (only the studies reported in [56, 59] are worthy of note along with the phenomenological analysis performed in [101])}; the problem of explaining, within the Green's function method, the upband found in the radiative strength function at energies below 3 MeV for many nuclei (see [53]); and the problem of testing the Brink–Axel hypothesis (this is possible upon performing cumbersome calculations aimed at an analysis of third-order anharmonic effects).

ACKNOWLEDGMENTS

We are grateful to the Organizing Committee of the 68th International Conference "Nucleus-2018" for providing us with the possibility of presenting this article in the form of a report at a plenary meeting of this conference. Of course, the results obtained in the theoretical studies performed within the period spanning 2012 and 2018 and quoted in [26–107] (see the list of references in the present article) could not be described in sufficient detail either in that report or in the present article. We are grateful to the authors of those articles for their contribution to the aforementioned studies and for enlightening discussions.

FUNGING

This work was supported by Russian Science Foundation (grant no. 16-12-10155).

REFERENCES

1. O. Bohr and B. Mottelson, *Nuclear Structure*, Vol. 2: *Nuclear Deformations*, (Benjamin, New York, 1975).
2. V. G. Soloviev, *Theory of Atomic Nuclei: Quasiparticle and Phonons* (Inst. Phys. Publ., Bristol, Philadelphia, 1992; Energoatomizdat, Moscow, 1989).
3. N. Paar, D. Vretenar, E. Khan, and G. Colo, Rep. Prog. Phys. **70**, 691 (2007).
4. D. Vretenar, A. V. Afanasjev, G. A. Lalazissis, and P. Ring, Phys. Rep. **409**, 101 (2005).
5. S. Goriely and E. Khan, Nucl. Phys. A **706**, 217 (2002).
6. V. A. Khodel and E. E. Saperstein, Phys. Rep. **92**, 183 (1982).
7. A. V. Smirnov, S. V. Tolokonnikov, and S. A. Fayans, Sov. J. Nucl. Phys. **48**, 995 (1988).
8. S. V. Tolokonnikov and E. E. Saperstein, Phys. At. Nucl. **73**, 1684 (2010).

9. P. Klüpfel, P.-G. Reinhard, T. J. Bürvenich, and J. A. Maruhn, Phys. Rev. C **79**, 034310 (2009).
10. P. Ring and J. Speth, Nucl. Phys. A **235**, 315 (1974).
11. V. A. Khodel', Sov. J. Nucl. Phys. **24**, 367 (1976).
12. A. B. Migdal, *Theory of Finite Fermi Systems and Applications to Atomic Nuclei* (Nauka, Moscow, 1965; Intersci., New York, 1967).
13. S. P. Kamerdzhiev, Sov. J. Nucl. Phys. **38**, 188 (1983).
14. V. I. Tselyaev, Sov. J. Nucl. Phys. **50**, 780 (1989).
15. S. Kamerdzhiev, J. Speth, and G. Tertychny, Phys. Rep. **393**, 1 (2004).
16. V. Tselyaev, Phys. Rev. C **75**, 024306 (2007).
17. Nguyen Van Giai, Ch. Stoyanov, and V. V. Voronov, Phys. Rev. C **57**, 1204 (1998).
18. S. P. Kamerdzhiev, A. V. Avdeenkov, and D. A. Voitenkov, Phys. At. Nucl. **74**, 1478 (2011).
19. S. V. Tolokonnikov, S. Kamerdzhiev, D. Voytenkov, S. Krewald, and E. E. Saperstein, Phys. Rev. C **84**, 064324 (2011).
20. A. Avdeenkov, S. Goriely, S. Kamerdzhiev, and S. Krewald, Phys. Rev. C **83**, 064316 (2011).
21. https://www.nndc.bnl.gov/ensdf/.
22. H. Grawe, K. Langanke, and G. Martinez-Pinedo, Rep. Prog. Phys. **70**, 1525 (2007).
23. K. Kitao, M. Kanbe, and K. Ogawa, Nucl. Data Sheets **67**, 327 (1992).
24. T. Tamura, H. Iimura, K. Miyano, and S. Ohya, Nucl. Data Sheets **64**, 323 (1991).
25. H. Wapstra and G. Audi, Nucl. Phys. A **432**, 55 (1985).
26. A. Avdeenkov and S. P. Kamerdzhiev, in *50 Years of Nuclear BCS,* Ed. by R. Broglia and V. Zelevinsky (World Scientific, Singapore, 2012), Chap. 20, p. 274.
27. S. Kamerdzhiev and E. E. Saperstein, Eur. Phys. J. A **37**, 333 (2008).
28. A. V. Avdeenkov and S. P. Kamerdzhiev, Phys. At. Nucl. **62**, 563 (1999).
29. M. Baldo, U. Lombardo, E. E. Saperstein, and M. V. Zverev, Phys. Rep. **391**, 261 (2004).
30. E. E. Saperstein and S. V. Tolokonnikov, Phys. At. Nucl. **79**, 1030 (2016).
31. E. E. Saperstein, M. Baldo, S. S. Pankratov, and S. V. Tolokonnikov, JETP Lett. **104**, 609 (2016).
32. N. V. Gnezdilov, E. E. Saperstein, and S. V. Tolokonnikov, Phys. At. Nucl. **78**, 24 (2015).
33. N. V. Gnezdilov, E. E. Saperstein, and S. V. Tolokonnikov, Eur. Phys. Lett. **107**, 62001 (2014).
34. N. V. Gnezdilov, I. N. Borzov, E. E. Saperstein, and S. V. Tolokonnikov, Phys. Rev. C **89**, 034304 (2014).
35. E. E. Saperstein, N. V. Gnezdilov, and S. V. Tolokonnikov, AIP Conf. Proc. **1619**, 145 (2014).
36. E. Litvinova, Phys. Rev. C **85**, 021303(R) (2012).
37. N. J. Stone, *Table of Nuclear Magnetic Dipole and Electric Quadrupole Moments* (IAEA, 2014).
38. S. P. Kamerdzhiev, O. I. Achakovskiy, D. A. Voitenkov, and S. V. Tolokonnikov, Phys. At. Nucl. **77**, 66 (2014).
39. E. E. Saperstein, O. I. Achakovskiy, S. P. Kamerdzhiev, S. Krewald, J. Speth, and S. V. Tolokonnikov, Phys. At. Nucl. **77**, 1033 (2014).
40. E. E. Saperstein, S. Kamerdzhiev, D. S. Krepish, S. V. Tolokonnikov, and D. Voitenkov, J. Phys. G **44**, 065104 (2017).
41. E. E. Saperstein, S. Kamerdzhiev, D. S. Krepish, S. V. Tolokonnikov, and D. Voitenkov, in *Proceedings of Conference ICNFP-2017*, arXiv: 1712.00982.
42. S. V. Tolokonnikov, S. Kamerdzhiev, S. Krewald, E. E. Saperstein, and D. Voitenkov, Eur. Phys. J. A **48**, 70 (2012).
43. E. E. Saperstein and S. V. Tolokonnikov, AIP Conf. Proc. **1912**, 020016 (2017).
44. V. Yu. Ponomarev, Ch. Stoyanov, N. Tsoneva, and M. Grinberg, Nucl. Phys. A **635**, 470 (1998).
45. D. Voitenkov, S. Kamerdzhiev, S. Krewald, E. E. Saperstein and S. V. Tolokonnikov, Phys. Rev. C **85**, 054319 (2012).
46. R. A. Broglia, R. Liotta, and V. Paar, Phys. Lett. B **38**, 480 (1972).
47. A. P. Platonov, Sov. J. Nucl. Phys. **36**, 492 (1982).
48. E. E. Saperstein, S. P. Kamerdzhiev, S. Krewald, J. Speth, and S. V. Tolokonnikov, JETP Lett. **98**, 631 (2013).
49. S. P. Kamerdzhiev and D. A. Voitenkov, Phys. At. Nucl. **79**, 904 (2016).
50. S. P. Kamerdzhiev, D. A. Voitenkov, E. E. Sapershtein, S. V. Tolokonnikov, and M. I. Shitov, JETP Lett. **106**, 139 (2017).
51. H. K. Toft, A. C. Larsen, A. Bürger, M. Guttormsen, A. Görgen, H. T. Nyhus, T. Renstrøm, S. Siem, G. M. Tveten, and A. Voinov, Phys. Rev. C **83**, 044320 (2011).
52. T. Renstrøm, G. M. Tveten, J. E. Midtbø, H. Utsunomiya, O. Achakovskiy, S. Kamerdzhiev, B. Alex Brown, A. Avdeenkov, T. Ari-izumi, A. Görgen, S. M. Grimes, M. Guttormsen, T. W. Hagen, V. W. Ingeberg, S. Katayama, B. V. Kheswa, et al., arXiv: 1804.08086v1.
53. A. C. Larsen, J. E. Midtbø, M. Guttormsen, T. Renstrøm, S. N. Liddick, A. Spyrou, S. Karampagia, B. A. Brown, O. Achakovskiy, S. Kamerdzhiev, D. L. Bleuel, A. Couture, L. Crespo Campo, B. P. Crider, A. C. Dombos, R. Lewis, et al., Phys. Rev. C **97**, 054329 (2018).
54. S. N. Liddick, A. Spyrou, B. P. Crider, F. Naqvi, A. C. Larsen, M. Guttormsen, M. Mumpower, R. Surman, G. Perdikakis, D. L. Bleuel, A. Couture, L. Crespo Campo, A. C. Dombos, R. Lewis, S. Mosby, et al., Phys. Rev. Lett. **116**, 242502 (2016).
55. M. Guttormsen, R. Chankova, U. Agvaanluvsan, E. Algin, L. A. Bernstein, F. Ingebretsen, T. Lönnroth, S. Messelt, G. E. Mitchell, J. Rekstad,

A. Schiller, S. Siem, A. C. Sunde, A. Voinov, and S. Ødegård, Phys. Rev. C **71**, 044307 (2005).
56. E. Litvinova, P. Ring, and V. I. Tselyaev, Phys. Rev. C **88**, 044320 (2013).
57. R. Schwengner, S. Frauendorf, and A. C. Larsen, Phys. Rev. Lett. **111**, 232504 (2013).
58. O. Wieland, A. Bracco, F. Camera, G. Benzoni, N. Blasi, S. Brambilla, F. C. L. Crespi, S. Leoni, B. Million, R. Nicolini, A. Maj, P. Bednarczyk, J. Grebosz, M. Kmiecik, W. Meczynski, and J. Styczen, Phys. Rev. Lett. **102**, 092502 (2009).
59. E. Litvinova, P. Ring, and V. I. Tselyaev, Phys. Rev. Lett. **105**, 022502 (2010).
60. S. P. Kamerdzhiev, A. V. Avdeenkov, and O. I. Achakovskiy, in *Proceedings of the All-Russia Seminar on Giant Dipole Resonance. Results and Prospects, Moscow, Feb. 6, 2014* (2014), p. 33.
61. S. P. Kamerdzhiev, A. V. Avdeenkov, and O. I. Achakovskiy, Phys. At. Nucl. **77**, 1303 (2014).
62. O. Achakovskiy, A. Avdeenkov, S. Goriely, S. Kamerdzhiev, S. Krewald, and D. Voitenkov, EPJ Web Conf. **93**, 01034 (2015).
63. O. I. Achakovskiy, A. V. Avdeenkov, S. P. Kamerdzhiev, and D. A. Voitenkov, in *Proceedings of the 22nd International Seminar on Interaction of Neutrons with Nuclei, ISINN-22* (Dubna, 2014), p. 207.
64. O. I. Achakovskiy, A. V. Avdeenkov, and S. P. Kamerdzhiev, in *Proceedings of the 22nd International Seminar on Interaction of Neutrons with Nuclei, ISINN-22* (Dubna, 2014), p. 213.
65. O. Achakovskiy, A. Avdeenkov, S. Goriely, S. Kamerdzhiev, and S. Krewald, Phys. Rev. C **91**, 034620 (2015).
66. O. I. Achakovskiy, S. P. Kamerdzhiev, and V. I. Tselyaev, JETP Lett. **104**, 374 (2016).
67. K. Wisshak, F. Voss, Ch. Theis, F. Käppeler, K. Guber, L. Kazakov, N. Kornilov, and G. Reffo, Phys. Rev. C **54**, 1451 (1996).
68. V. M. Timokhov, M. V. Bokhovko, M. V. Isakov, L. E. Kazakov, V. N. Kononov, G. N. Manturov, E. D. Poletaev, and V. G. Pronyaev, IPPE Report No. 1921 (A. I. Leypunsky Inst. Phys. Power Eng., Obninsk, 1988).
69. M. Herman, R. Capote, B. V. Carlson, P. Obložinský, M. Sin, A. Trkov, H. Wienke, and V. Zerkin, Nucl. Data Sheets **108**, 2655 (2007).
70. R. Capote, M. Herman, P. Obložinský, P. G. Young, S. Goriely, T. Belgya, A. V. Ignatyuk, A. J. Koning, S. Hilaire, V. A. Plujko, M. Avrigeanu, O. Bersillon, M. B. Chadwick, T. Fukahori, Zhigang Ge, Yinlu Han, et al., Nucl. Data Sheets **110**, 3107 (2009).
71. T. Belgya, O. Bersillon, R. Capote, T. Fukahori, Ge Zhigang, S. Goriely, M. Herman, A. V. Ignatyuk, S. Kailas, A. J. Koning, P. Obložinský, V. Plujko, and P. G. Young, IAEA-TECDOC-1506 (IAEA, Vienna, 2006).
72. S. Goriely, S. Hilaire, and A. J. Koning, Phys. Rev. C **78**, 064307 (2008).
73. S. Goriely, E. Khan, and V. Samyn, Nucl. Phys. A **739**, 331 (2004).
74. O. Achakovskiy, A. Avdeenkov, and S. Kamerdzhiev, EPJ Web Conf. **107**, 05002 (2016).
75. O. Achakovskiy, S. Kamerdzhiev, V. Tselyaev, and M. Shitov, EPJ Web Conf. **107**, 05005 (2016).
76. S. P. Kamerdzhiev, O. I. Achakovskiy, and A. V. Avdeenkov, JETP Lett. **101**, 725 (2015).
77. S. P. Kamerdzhiev, O. I. Achakovskiy, A. V. Avdeenkov, and S. Gorieli, Phys. At. Nucl. **79**, 567 (2016).
78. S. F. Mughabghab, *Atlas of Neutron Resonances, Resonance Parameters, and Thermal Cross Sections $Z = 1–100$* (Elsevier, Amsterdam, 2006).
79. S. P. Kamerdzhiev and S. F. Kovalev, Phys. At. Nucl. **69**, 418 (2006).
80. O. Achakovskiy and S. Kamerdzhiev, EPJ Web of Conf. **146**, 05003 (2017).
81. I. Poltoratska, P. von Neumann-Cosel, A. Tamii, T. Adachi, C. A. Bertulani, J. Carter, M. Dozono, H. Fujita, K. Fujita, Y. Fujita, K. Hatanaka, M. Itoh, T. Kawabata, Y. Kalmykov, A. M. Krumbholz, E. Litvinova, et al., Phys. Rev. C **85**, 041304(R) (2012).
82. N. Lyutorovich, V. I. Tselyaev, J. Speth, S. Krewald, F. Grümmer, and P.-G. Reinhard, Phys. Rev. Lett. **109**, 092502 (2012).
83. V. Tselyaev, N. Lyutorovich, J. Speth, S. Krewald, and P.-G. Reinhard, Phys. Rev. C **94**, 034306 (2016).
84. N. U. H. Syed, M. Guttormsen, F. Ingebretsen, A. C. Larsen, T. Lönnroth, J. Rekstad, A. Schiller, S. Siem, and A. Voinov, Phys. Rev. C **79**, 024316 (2009).
85. N. Ryezayeva, T. Hartmann, Y. Kalmykov, H. Lenske, P. von Neumann-Cosel, V. Yu. Ponomarev, A. Richter, A. Shevchenko, S. Volz, and J. Wambach, Phys. Rev. Lett. **89**, 272502 (2002).
86. A. Tamii, I. Poltoratska, P. von Neumann-Cosel, Y. Fujita, T. Adachi, C. A. Bertulani, J. Carter, M. Dozono, H. Fujita, K. Fujita, K. Hatanaka, D. Ishikawa, M. Itoh, T. Kawabata, Y. Kalmykov, A. M. Krumbholz, et al., Phys. Rev. Lett. **107**, 062502 (2011).
87. M. N. Harakeh and A. E. L. Dieperink, Phys. Rev. C **23**, 2329 (1981).
88. T. D. Poelhekken, S. K. B. Hesmondhalgh, H. J. Hofmann, A. van der Woude, and M. N. Harakeh, Phys. Lett. B **278**, 423 (1992).
89. S. N. Belyaev, O. V. Vasil'ev, V. V. Voronov, A. A. Nechkin, V. Yu. Ponomarev, and V. A. Semenov, Phys. At. Nucl. **58**, 1833 (1995).
90. N. A. Lyutorovich, V. I. Tselyaev, O. I. Achakovskiy, and S. P. Kamerdzhiev, JETP Lett. **107**, 659 (2018).
91. V. Tselyaev, N. Lyutorovich, J. Speth, and P.-G. Reinhard, Phys. Rev. C **96**, 024312 (2017).

92. P. Ring, E. Litvinova, and V. Tselyaev, AIP Conf. Proc. **1491**, 214 (2012).
93. N. Lyutorovich, V. Tselyaev, J. Speth, S. Krewald, and P.-G. Reinhard, Phys. At. Nucl. **79**, 868 (2016).
94. J. Speth and N. Lyutorovich, Int. J. Mod. Phys. E **26**, 1740025 (2017).
95. V. Tselyaev, N. Lyutorovich, J. Speth, and P.-G. Reinhard, Phys. Rev. C **97**, 044308 (2018).
96. V. I. Tselyaev, AIP Conf. Proc. **1606**, 201 (2014).
97. V. I. Tselyaev, Phys. Rev. C **88**, 054301 (2013).
98. E. Litvinova and V. I. Tselyaev, in *Fifty Years of Nuclear BCS: Pairing in Finite Systems* (World Scientific, Singapore, 2013), Chap. 10, p. 125.
99. J. Speth, S. Krewald, F. Grümmer, P.-G. Reinhard, N. Lyutorovich, and V. Tselyaev, Nucl. Phys. A **928**, 17 (2014).
100. N. Lyutorovich, V. Tselyaev, J. Speth, S. Krewald, F. Grümmer, and P.-G. Reinhard, Phys. Lett. B **749**, 292 (2015).
101. S. P. Kamerdzhiev and V. N. Tkachev, Sov. J. Nucl. Phys. **36**, 43 (1982).
102. E. E. Saperstein, S. Kamerdzhiev, S. Krewald, J. Speth, and S. V. Tolokonnikov, Eur. Phys. Lett. **103**, 42001 (2013).
103. E. E. Saperstein, M. Baldo, S. S. Pankratov, and S. V. Tolokonnikov, JETP Lett. **106**, 555 (2017).
104. E. E. Saperstein, M. Baldo, S. S. Pankratov, and S. V. Tolokonnikov, JETP Lett. **104**, 743 (2016).
105. E. E. Saperstein, M. Baldo, N. V. Gnezdilov, and S. V. Tolokonnikov, Phys. Rev. C **93**, 034302 (2016).
106. E. E. Saperstein, M. Baldo, N. V. Gnezdilov, and S. V. Tolokonnikov, JETP Lett. **103**, 1 (2016).
107. S. Kamerdzhiev, D. Voitenkov, E. E. Saperstein, and S. V. Tolokonnikov, JETP Lett. **108**, 155 (2018).